ION-MOBILITY MASS SPECTROMETRY OF COMPLEXES OF NICKEL AND ACETONITRILE

Detlef SCHRÖDER

Institute of Organic Chemistry and Biochemistry, Academy of Sciences of the Czech Republic, v.v.i., Flemingovo nám. 2, 16610 Prague 6, Czech Republic; e-mail: detlef.schroeder@uochb.cas.cz

Received January 25, 2011
Accepted February 25, 2011
Published online April 1, 2011

Dedicated to Dr. Zdeněk Havlas on the occasion of his 60th birthday.

Mono- and dications of microsolvated nickel complexes of acetonitrile are probed by means of ion-mobility mass spectrometry. Specifically, the complexes $[(CH_3CN)_nNi]^+$, $[(CH_3CN)_nNi]^{2+}$, $[(CH_3CN)_nNiOH]^+$, and $[(CH_3CN)_nNiCl]^+$ (n = 0–6) are compared to each other and their reactions with background water are probed. In general, the arrival times of the ions in the ion-mobility experiment linearly increase with the mass-to-charge ratio, but for the smaller, more reactive complexes, the arrival times are notably larger than expected from their mass. This effect is attributed to the markedly larger reactivity of these particular ions, as reflected in both charge-separation processes as well as adduct formation upon interaction with background water.

Keywords: Acetonitrile; Dications; Electrospray ionization; Ion mobility mass spectrometry; Nickel.

About a decade ago, Rulíšek and Havlas investigated the coordination chemistry of 3d-transition-metal dications in a series of seminal papers. Starting with simple organic and inorganic ligands[1,2] they went on to more complex biomolecules[3–6], and still today their investigations receive broad attention of coordination chemists. In about the same period, the gas-phase chemistry of ligated metal dications[7–9] has experienced a boost due to the development of electrospray ionization (ESI) mass spectrometry[10]. As being among the most popular solvents in organic synthesis and analytical chemistry, acetonitrile has often been chosen as a ligand and numerous complexes of the type $[(CH_3CN)_nM]^{2+}$ have been investigated using ESI-MS [11–21]. For some trivalent metals, even the formation of free, triply charged complexes with acetonitrile in the gas phase have been reported[22]. Upon transfer of such ions from solution to the gas phase, solvation is of crucial

Collect. Czech. Chem. Commun. 2011, Vol. 76, No. 5, pp. 351–369

doi:10.1135/cccc2011020

importance for the relationship between the formal oxidation state of the metal and the real Coulomb charge of the complexes[23].

$$MX_{2,solv} \rightarrow MX^{+}_{solv} + X^{-}_{solv} \quad (1)$$

$$MX^{+}_{solv} \rightarrow M^{2+}_{solv} + X^{-}_{solv} \quad (2)$$

$$M^{2+}_{solv} + H_2O \rightarrow MOH^{+}_{solv} + H^{+}_{solv} \quad (3)$$

In a dipolar solvent, a salt of a divalent metal MX_2 (X = monovalent counterion such as Cl etc.) undergoes heterolytic dissociation according to reactions (*1*) and (*2*) to afford mono- and dicationic species which can be detected by ESI-MS in the positive ion mode. In the presence of water, the solvated dications can also recombine with a hydroxide ion to form monocationic hydroxo complexes in conjunction with the liberation of protons (reaction (*3*)). The ratio between the MX^{+}_{solv} and M^{2+}_{solv} ions depends on the nature of the counterion X, the concentration of the solution, and the ionization conditions. The extent of reaction (*3*) obviously depends on the amount of water being present. In general, poorly coordinating counterions, e.g. ClO_4^-, increase the dication yields, whereas better coordinating anionic ligands give significant amounts of the monocations MX^{+}_{solv} (e.g. X = Cl). In a first approximation, the total concentration of the metal salt in solution affects the $MX^{+}_{solv}/M^{2+}_{solv}$ ratio via the mass-action law in that ion-pairing[24] is more pronounced at higher concentrations and hence associated with an increase of MX^{+}_{solv} [25,26]. The ionization conditions crucially influence the amount of microsolvation of the ions formed[27,28]. At soft conditions of ionization (i.e. low source temperature and gentle focusing potentials), highly solvated ions are formed, even including species with second solvation shells[29,30]. At higher temperatures or with an increasing amount of energizing collisions due to elevated potentials in the source region, the ionization conditions become harder, leading to partial or even complete desolvation of the initial ions. By tuning the various parameters, a manifold of ions ranging from large solvate clusters to atomic cations is therefore accessible via electrospray ionization for more detailed investigations in subsequent mass-spectrometric experiments[28,29,31,32].

Here, we describe gas-phase experiments on several cationic nickel complexes with acetonitrile as a solvating ligand[33]. As precursors for the electrospray ionization studies, we use a solution of $Ni(ClO_4)_2$ in acetonitrile and a solution of $NiCl_2$ in water/acetonitrile (2:1) from which the fol-

lowing ions can be prepared in yields sufficient for subsequent studies: $[(CH_3CN)_nNi]^+$ (n = 1–3), $[(CH_3CN)_nNiOH]^+$ (n = 1–3), $[(CH_3CN)_nNiCl]^+$ (n = 0–3), and $[(CH_3CN)_nNi]^{2+}$ (n = 2–6). Note that the formal nickel(I) species $[(CH_3CN)_nNi]^+$ are formed in charge-separation reactions of the $[(CH_3CN)_nNi]^{2+}$ dications at enforced ionization conditions (reaction (*4*))[15,21].

$$[(CH_3CN)_nNi]^{2+} \rightarrow [(CH_3CN)_{n-1}Ni]^+ + CH_3CN^+ \qquad (4)$$

The ions were investigated using ion-mobility mass spectrometry (IM-MS) with which not only ion masses, but also their apparent cross section in the interaction with a quasi-inert gas can be probed[34–36]. Although this technique itself is already quite old, it only recently found wide applications due to the introduction of a commercial instrument. Therefore, it appears appropriate to briefly introduce the method which involves three crucial steps: (i) ion generation, mass selection and accumulation, (ii) injection of these ions at a given time (t = 0) into a mobility cell in which a non-reactive gas (here nitrogen) is present at a pressure in the mbar range, while an accumulative potential gradient is used to maintain the forward movement of the ions, and (iii) time-dependent extraction, mass analysis and ion detection which leads to arrival time distributions (ATDs) for each ion mass. Depending on the ions' mass-to-charge ratio (m/z) and their interactions with the gas in the mobility cell, the ions reach the detector at different arrival times (t_a), where small and light ions are faster than large and heavy species. To a first approximation, ion mobility of gaseous ions may be compared to chromatography in the condensed phase. In this analogy, the electric field gradient serves as mobile phase and nitrogen acts as the stationary phase and providing a resistance against forward-transport of the ions. For two isobaric ions of different shape ("potato and cigar"), the more compact one interacts less with the buffer gas and thus arrives earlier at the detector than the more extended ion of identical mass. Therefore, IM-MS provides the molecular shape as a additional dimension in mass spectrometry. So far, IM-MS has mostly been used for either atomic systems or rather large molecules and most present applications are in the area of biomolecules and polymers, whereas small or medium-sized molecules were much less often studied using IM-MS [34–36]. Here, we report about first results of this interesting technique when used for the investigation of medium-sized microsolvated transition-metal complexes. As demonstrated below, quite significant deviations from the typical behavior of ions in IM-MS are observed for coordinatively significantly unsaturated metal complexes.

EXPERIMENTAL

The experiments were performed with a SYNAPT G2 ion-mobility instrument[37,38]. In brief, the instrument has an ESI source from which the ions are extracted towards a quadrupole mass filter for the selection of parent ions. In the ion-mobility mode, the mass-selected ions enter an argon-filled linear ion trap in which they are collected and then admitted in pulses via a helium cooling cell to a drift tube in which nitrogen is present at an approximate pressure of 2 mbar. After extraction from the drift tube, the ions pass a transfer cell and enter the source region of a reflectron time-of-flight (TOF) mass spectrometer, which quasi continuously records mass spectra with a mass resolution ($m/\Delta m$) of ca. 25000. In the ion-mobility experiments described below, the desired $[(CH_3CN)_nNiX]^{+/2+}$ cations (n = 0–5, X = none, OH, Cl) were mass-selected using Q1 at unit mass resolution and the ion mobility was recorded in time steps of about 0.05 ms required for recording and processing TOF spectra from m/z 50 to 1200. In order to minimize fragmentation of more weakly bound complexes, the potentials in ion transfer to the drift cell were lowered as much as possible, while still maintaining acceptable ion transmission[39]. For a given ion of interest, the amount of fragmentation can in each case still be lowered significantly, but this procedure critically depends on the bias voltage of the linear ion trap which turns out to be mass-sensitive, however. Accordingly, a compromise between the amount of fragmentation and transmission of the ions in the mass range investigated (m/z 70–216) was chosen. The elemental composition of all ions was confirmed by examination of the associated isotope envelopes in the source spectra and the exact ion masses which had an average error of 0.0006 amu compared to the theoretical masses with maximal deviations of 0.0014 amu in the cases of $[(CH_3CN)_2Ni]^{2+}$ and $[(CH_3CN)NiCl]^+$. Note that the high mass resolution of the back-end TOF detector often allows to separately follow the various ions even if nominally isobaric ions not resolved by Q1 may interfere.

It is important to note that the absolute values of the arrival times in the SYNAPT G2 very much depend on the adjustments of the pressures and the voltage settings. Any comparison can therefore only be made relative to each other under identical settings. For a given set of gas flows and voltages, however, the arrival times are quite well reproducible and do not show day-to-day variations or similar imponderable effects. Further noteworthy is that significant amounts of the solvent used in the ESI source may diffuse into the mobility section and give rise to association processes and charge-separation reactions in the case of gaseous dications (see below). While the amounts of the more volatile acetonitrile in the mobility unit were found to be almost negligible, water can obviously reach this region better[28]. Moreover, the amount of water also depends on the history of the machine: when switching from pure water for overnight cleaning to a solution of $Ni(ClO_4)_2$ in pure acetonitrile, the amount of water present in the mobility cell is first quite large and then slowly decreases during several hours. For this reason, we refrain from a strictly quantitative analysis of the reactions observed with background water, while relative comparisons between different ions generated from a certain solution in a short period of time can still be made.

As precursors for ion generation, 10^{-3} M solutions of $Ni(ClO_4)_2$ (Fluka) and $NiCl_2$ (Sigma–Aldrich), respectively, in HPLC-grade acetonitrile (Sigma–Aldrich) or water/acetonitrile (2:1) were used, which were infused to the ESI at a flow rate of 5 μl min^{-1}. The desolvation temperature was 200 °C and the ESI source was kept at 80 °C to avoid contamination.

RESULTS AND DISCUSSION

A central part of the discussion will concern reactions occurring within the ion-mobility set-up which are manifested in the mass spectra as well as the arrival time distributions. Therefore, prior to the presentation of the results for the cationic nickel complexes of acetonitrile, it is considered necessary to outline the basic features of the experiment. The general scheme of the instrument is shown in Fig. 1.

When operating in the IM-MS mode, the ions generated in the ESI source are transferred to the vacuum manifold using a traveling wave guide which can optionally be filled with argon for cooling. Then, the ion of interest is mass-selected using the quadrupole analyzer Q1, the ions are collected in a linear ion trap filled with argon from which they are injected as a single pulse at $t_a = 0$ via a helium cell to the ion-mobility separator (IMS) in which nitrogen is present at a pressure of about 2 mbar. Depending on the mass-to-charge ratio and the interaction with the nitrogen, the ions need different times for the passage of the IMS which are reflected in their arrival times (t_a) at the detector. Afterwards, the ions reach a transfer cell filled with argon in which they are stored for short time intervals before being directed into a reflectron time-of-flight mass spectrometer recording a mass spectrum. 200 of these TOF spectra are taken in each duty cycle and these serve as the time axis for ion mobility. The set of TOF mass spectra permits the construction of various ion-mobility graphs with the dimensions ion mass, arrival time, and intensity.

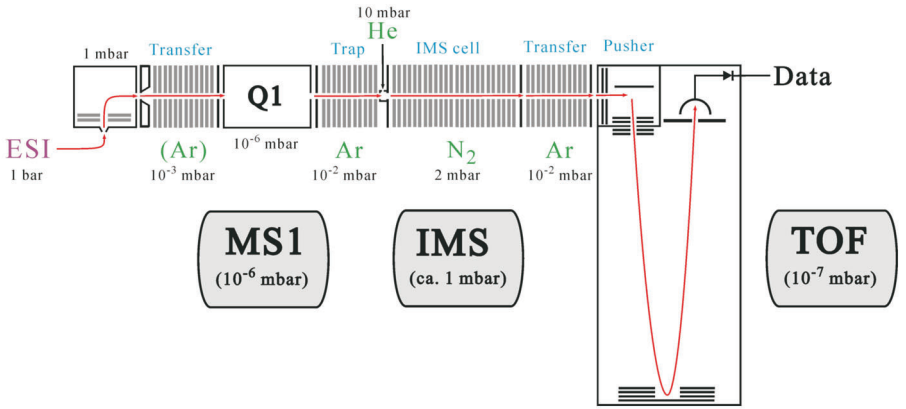

FIG. 1
Schematic set-up of the SYNAPT G2 instrument used for ion-mobility mass spectrometry: Q, quadrupole analyzer; IMS, ion-mobility separator; TOF, time-of-flight mass spectrometer

For illustration, let us consider a hypothetical experiment conducted with three different ions: a light (red) and a heavier (green) ion with similar sizes and an extended ion (purple) isobaric to the heavier one. Scheme 1a shows the effect of the *m/z* ratio which is due to the fact that at a given setting of the potential gradient in the IMS cell, the lighter ion moves faster than the heavier one and thus the former arrives first at the detector and has a smaller t_a. Scheme 1b illustrates the situation of two isobaric ions of different shapes, where the more compact (green) ion interacts less with the nitrogen gas in the IMS cell and thus travels faster than the more extended (purple) ion which collides more often and thus arrives at a larger t_a. When all ions are admitted to the IMS unit (i.e. no mass selection in Q1), a three-dimensional representation as shown in Scheme 1c is obtained.

In the case of small or medium-sized molecules, there arises an additional problem, however, which is inherent to the conception of the IM-MS experiment. Specifically, ion extraction from the source and mass selection in the quadrupole require the ions to be accelerated to some non-zero voltage to allow proper manipulation. When entering the IMS region, these ions thus exhibit excess kinetic energy relative to the gases in the trap, mobility and transfer cells. Neither for atoms nor for large molecules the resulting conversion of kinetic into heat really matters, but small or medium-sized molecules can undergo collision-induced dissociation (CID).

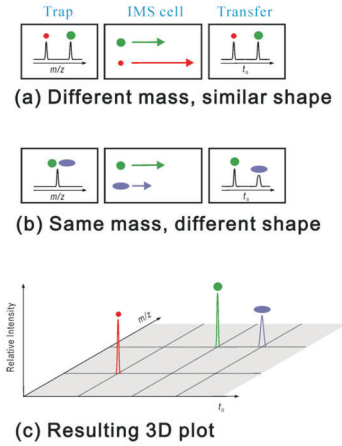

SCHEME 1
Sketch of the IMS separation for ions of different mass and similar shape (a), isobaric ions of different shape (b), and the corresponding 3D plot (c)

As shown further below, also other chemical reactions can occur during the passage of the mobility cell, which turn out to be of crucial importance for the nickel/acetonitrile complexes with low coordination numbers. Therefore, let us consider a second hypothetical scenario in which an ion AB^+ and its fragment A^+ are sampled via IM-MS. In the absence of fragmentation or other chemical reactions, a single peak is obtained in both the mobility and the mass spectrum (Scheme 2a). If ion dissociation occurs in the trap prior to the IMS unit, the parent AB^+ and the daughter A^+ enter the IMS cell at $t_a = 0$ and the lighter and smaller fragment A^+ will reach the detector first (Scheme 2b). In the case that the fragmentation occurs at some stage of the IMS separation, the apparent ion mobility of A^+ is in-between those of AB^+ and A^+. Assuming that the propensity for dissociation is the same in the entire IMS cell, this will lead to non-zero baseline between $t_a(A^+)$ and $t_a(AB^+)$ as shown in Scheme 2c. Dissociation upon transfer will show up in the mass spectra, but not in the mobility trace because only intact AB^+ passed the IMS cell (Scheme 2d). In the resulting ion-mobility spectra including all three options in Schemes 2b–2d, AB^+ shows a single peak, because any fragments would appear at different masses (Scheme 2e). Instead, the trace of the fragment A^+ has three components (Scheme 2f), an early from dissociation in the trap, a raised baseline from fragmentation within the IMS, and a late peak due to fragmentation of intact AB^+ upon transfer. Similar arguments can be used to explain the effects observed when ion association, hence formation of heavier ions, occurs in the mobility step.

After having introduced the experimental technique, the dication $[(CH_3CN)_3Ni]^{2+}$ (*m/z* 90.5 for the ^{58}Ni isotope) is considered in more detail as an example, in order to illustrate the kind of information achieved in

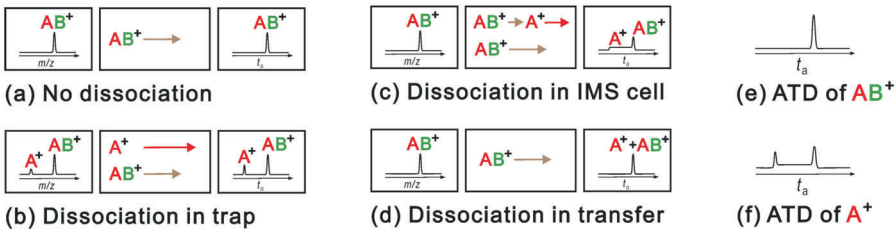

SCHEME 2
Sketch of the consequences of ion dissociation within different parts of the IMS unit and the resulting arrival time distributions of the hypothetical parent ion AB^+ and its ionic fragment A^+

IM-MS measurements. As outlined above, a significant amount of fragmentation is observed upon injection of mass-selected $[(CH_3CN)_3Ni]^{2+}$ into the mobility unit which leads to the smaller dication $[(CH_3CN)_2Ni]^{2+}$ at *m/z* 70 according to reaction (*5*) and is indicated by a red arrow in Fig. 2. Traces of water present in the mobility unit lead to sequential additions of water to the various dications (reaction (*6*)) with m = 1, 2 for n = 2, 3) as indicated by the blue arrows in Fig. 2.

From the intensity patterns of the microhydrated $[(CH_3CN)_n Ni(H_2O)_m]^{2+}$ dications it is obvious that the affinity for water addition is much larger for the dication with two only acetonitrile ligands compared to that with n = 3, i.e. $[(CH_3CN)_2Ni(H_2O)]^{2+}$ is more abundant than $[(CH_3CN)_2Ni]^{2+}$, whereas $[(CH_3CN)_3Ni(H_2O)]^{2+}$ is less than half of $[(CH_3CN)_3Ni]^{2+}$ in the blue spectrum of Fig. 2. A third type of reaction involves charge separation concomitant with proton transfer (PT) to yield the monocationic nickel hydroxo complexes $[(CH_3CN)_n NiOH]^+$ (reactions (*7*) and (*7a*))[40]; in the low mass range, the concomitant protonated acetonitrile has been observed also (m_{exp} = 42.0349, m_{calc} = 42.0344). In Fig. 2, the color code of these three different type of pathways is red for the collision-induced loss of acetonitrile, blue for the association with water, and green for the proton-transfer channel of the dication to the hydroxo monocations.

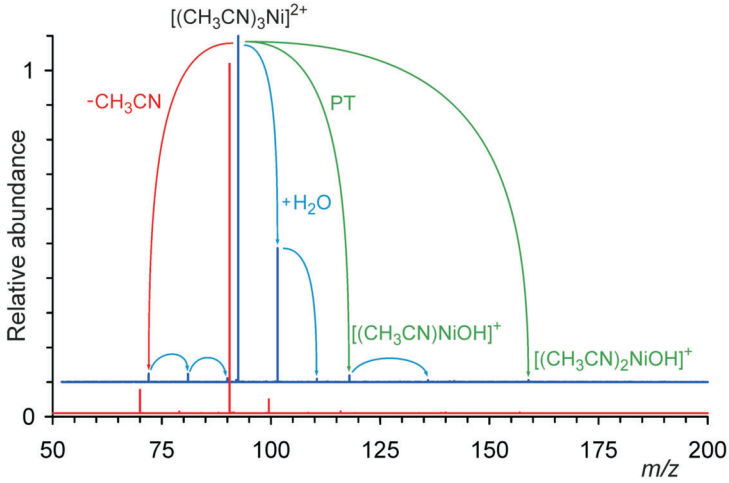

FIG. 2
Mass spectra resulting from injection of mass-selected $[(CH_3CN)_3Ni]^{2+}$ (*m/z* 90.5 for ^{58}Ni) into the ion-mobility cell. The red spectrum was obtained from $Ni(ClO_4)_2$ dissolved in pure acetonitrile and the blue spectrum from $NiCl_2$ solution in water/acetonitrile (2:1)

$$[(CH_3CN)_3Ni]^{2+} \rightarrow [(CH_3CN)_2Ni]^{2+} + CH_3CN \quad (5)$$

$$[(CH_3CN)_nNi]^{2+} + m\ H_2O \rightarrow [(CH_3CN)_nNi(H_2O)_m]^{2+} \quad (6)$$

$$[(CH_3CN)_3Ni]^{2+} + H_2O \rightarrow [(CH_3CN)_2NiOH]^{+} + CH_3CNH^{+} \quad (7)$$

$$[(CH_3CN)_3Ni]^{2+} + H_2O \rightarrow [(CH_3CN)NiOH]^{+} + CH_3CNH^{+} + CH_3CN \quad (7a)$$

The assignment of these reactions to the presence of water is further supported by the same experiment conducted with the precursor ion not generated form $Ni(ClO_4)_2$ in acetonitrile (red spectrum in Fig. 2), but from $NiCl_2$ in water/acetonitrile (blue spectrum in Fig. 2). Obviously, a notable amount of the water used as a solvent in electrospray can diffuse into the mobility section (see experimental details). Comparison of the red and blue spectra demonstrates that the water does not stem from the mobility unit itself, because the interference is minor when pure acetonitrile is used as a solvent. Interesting to note is that the effect is much smaller for the more volatile acetonitrile in that upon magnification only a very small signal corresponding to the adduct $[(CH_3CN)_4Ni]^{2+}$ can be observed in the red spectrum of Fig. 2, suggesting that the more sticky water is more likely to diffuse into the difference components of the vacuum system[28,41].

Next let us consider the associated arrival time distributions of the ions formed in this particular experiment which are recorded parallel to the mass spectra. Thus, each trace in Fig. 3 shows the intensity of selected ion(s) as a function of arrival time. The parent ion $[(CH_3CN)_3Ni]^{2+}$ has a nearly Gaussian-type ATD at t_a = 5.43 ms with a slight tailing to larger arrival times. The water adducts $[(CH_3CN)_3Ni(H_2O)_m]^{2+}$ (m = 1, 2) also peak at t_a = 5.43 ms, but their tailing to larger arrival times is more pronounced (label **a** in Fig. 3). This tailing effect is attributed to significant interactions of these dications with traces of water being present in the mobility cell which lead to the formation of transient adducts $[(CH_3CN)_3Ni(H_2O)_m]^{2+}$ ($m > 2$) which move slower in the mobility cell, but dissociate prior to detection. Tailing, rather than a distinct peak in the mobility trace, is a direct consequence of the fact that most collisions in the IMS occur with nitrogen gas and only traces of water interfere. Accordingly, one might expect a better separation in the IMS, if only water were used as an interacting partner. This favorable effect has indeed been observed in the separation of protonated amino ac-

ids upon addition of polar additives[42]. In the present case, however, it would obviously lead to exclusive association for the more reactive, coordinatively unsaturated nickel complexes and is thus obsolete. The $[(CH_3CN)_2Ni(H_2O)_m]^{2+}$ (m = 0–2) dications formed upon loss of one acetonitrile ligand from the parent have a composite ATD, where the component labeled **b** peaks peak at t_a = 5.43 ms like the parent ion itself and mostly comprises the non-hydrated fragment $[(CH_3CN)_2Ni]^{2+}$. In contrast, the second component at t_a = 5.81 ms is mostly composed of the microhydrates $[(CH_3CN)_2Ni(H_2O)_m]^{2+}$ (m = 1, 2). The products of proton transfer according to reaction (*7*) show a very broad distribution of arrival times which has an onset like the parent ion, peaks at t_a = 5.81 ms (label **c**) and vanishes at about t_a = 7.22 ms (label **d**), which corresponds to the arrival time of independently sampled $[(CH_3CN)_2NiOH]^+$ (see below). The broad distribution of the latter products illustrates the concepts outlined in Scheme 2 in that reaction (*7*) can occur in all parts of the mobility unit thereby leading to a nearly plateau-type feature.

After the detailed discussion of the results for $[(CH_3CN)_3Ni]^{2+}$, the data obtained for the other $[(CH_3CN)_nNi]^{2+}$ dications accessible from $Ni(ClO_4)_2$ in acetonitrile are given in Table I in a summarized form, where the fractions x_i refer to the contributions of the separate channels with $\Sigma x_i = 1$. Spe-

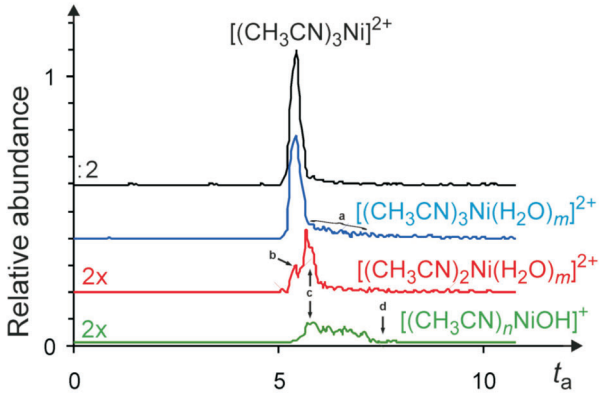

FIG. 3

Arrival time distributions upon injection of mass-selected $[(CH_3CN)_3Ni]^{2+}$ (*m/z* 90.5 for ^{58}Ni) into the ion-mobility cell. The upper black trace shows the parent ion, the blue trace the sum of the water adducts $[(CH_3CN)_3Ni(H_2O)_m]^{2+}$ (m = 1, 2), the red trace represents the sum of the bisacetonitrile complexes $[(CH_3CN)_2Ni(H_2O)_m]^{2+}$ (m = 0–2), and the green trace the hydroxo monocations $[(CH_3CN)_n(H_2O)_mNiOH]^+$ (m = 0, 1; n = 1, 2). The data refer to the experiment with a $NiCl_2$ solution in water/acetonitrile (2:1) as a precursor (blue spectrum in Fig. 2)

cifically, x_{parent} stands for the fraction of the mass-selected parent ion $[(CH_3CN)_nNi]^{2+}$ which is recovered from the ion-mobility cell, x_{CID} summarizes the abundances of the fragment ions formed via loss of acetonitrile, x_{ass} denotes the associations with background water to form $[(CH_3CN)_n{-}Ni(H_2O)_m]^{2+}$ (m = 1, 2 for n = 3 and m = 1 for n = 4), and x_{PT} stands for the proton-transfer channel to afford $[(CH_3CN)_{n'}NiOH]^+$ monocations ($n' < n$) according to reaction (*7*). All conclusions derived from the data shown in Table I are further supported by the associated ATD of the various parent and product ions in analogy to Fig. 3. However, for the sake of brevity in presentation, we restrict ourselves to a summary of the key results in the form of a table.

Although in these experiments pure acetonitrile was used as a solvent, the bisligated dication $[(CH_3CN)_2Ni]^{2+}$ shows a very high affinity to water, resulting in either addition to afford the dications $[(CH_3CN)_2Ni(H_2O)_m]^{2+}$ (m = 1, 2) at *m/z* 79.0 and 88.0, respectively, or charge separation concomitant with proton transfer to afford $[(CH_3CN)NiOH]^+$ at *m/z* 116. Interestingly, the arrival time of $[(CH_3CN)_2Ni]^{2+}$ (t_a = 5.61 ms) is somewhat larger than those for $[(CH_3CN)_3Ni]^{2+}$ and $[(CH_3CN)_4Ni]^{2+}$ to which we return further below. In comparison to the bisligated species $[(CH_3CN)_2Ni]^{2+}$, the trisligated dication $[(CH_3CN)_3Ni]^{2+}$, discussed in detail above (Figs 2 and 3), is much less reactive and the spectrum is dominated by the intact parent

TABLE I

Summarized results from the ion-mobility studies of mass-selected $[(CH_3CN)_nNi]^{2+}$ dications (n = 2–6) generated from a 10^{-3} M solution of $Ni(ClO_4)_2$ in pure acetonitrile with the molar fractions[a] x_i of the parent ion, the dicationic fragments formed by loss of acetonitrile[b], the adducts due to association with water, and the monocations $[(CH_3CN)_{n'}NiOH]^+$ formed via proton transfer in the mobility cell. Further, the arrival times (in ms) of the mass-selected parent ions are given

Parent ion	n	*m/z*	x_{parent}	x_{CID}[b]	x_{ass}	x_{PT}[c]	t_a(parent)
$[(CH_3CN)_nNi]^{2+}$	2	70.0	0.24	0.03	0.29	0.44	5.61
	3	90.5	0.90	0.06	0.03	0.01	5.34
	4	111.0	0.44	0.55		0.01	5.09
	5	131.5	0.01	0.98		0.01	5.94
	6	152.0	–[d]	0.99		0.01	–[d]

[a] Molar fractions with $\Sigma x_i = 1$. [b] This column includes exchange of one acetonitrile ligand by water. [c] For all ions, the predominating product of hydrolysis is $[(CH_3CN)NiOH]^+$ (*m/z* 116). [d] No intact *m/z* 152.0 detected.

ion with t_a = 5.34 ms. Collision-induced dissociation (CID) becomes of considerable importance for the larger members $[(CH_3CN)_nNi]^{2+}$ with $n > 3$. For $n = 4$ (t_a = 5.09 ms), more than half of the incident ions undergo CID, almost complete fragmentation to smaller $[(CH_3CN)_{n'}Ni]^{2+}$ dications occurs for $n = 5$ (t_a = 5.94 ms), and for $[(CH_3CN)_6Ni]^{2+}$ no transmission of the intact dication is observed at all. In fact, the mass spectra of $[(CH_3CN)_nNi]^{2+}$ with n = 4–6 are almost identical to each other with the major signals due to $[(CH_3CN)_3Ni]^{2+}$ and $[(CH_3CN)_4Ni]^{2+}$. This finding indicates that the ion-mobility experiment has a lower stability limit when it comes to multiply solvated ions. As far as the arrival times are concerned, the expected mass-dependence is only obeyed by $[(CH_3CN)_4Ni]^{2+}$ and $[(CH_3CN)_5Ni]^{2+}$, whereas the two smaller dications are less mobile than expected from their mere mass (see below).

In order to increase the database for understanding the ion mobilities, a solution of $NiCl_2$ in water/acetonitrile was used as an additional precursor. Depending on the conditions in the ion source, this solution provides simultaneous access to the dications $[(CH_3CN)_nNi]^{2+}$ (except $n = 2$) as well as various monocations such as the chloro complexes $[(CH_3CN)_nNiCl]^+$, the hydroxo complexes $[(CH_3CN)_nNiOH]^+$, and the nickel(I) species $[(CH_3CN)_nNi]^+$; the latter are only formed at harder conditions of ionization and are thus not due to possible electrochemical processes occurring in solution[43], but to CID of the dications according to reaction (*4*)[15,44–46]. The rich data obtained in the mobility experiments are summarized in Table II, in which we again restrict the presentation to the key information while the individual ATD traces of the various ions fully support the conclusions derived. Further note that in comparison to Table I, the arrival times of the $[(CH_3CN)_nNi]^{2+}$ dications are slightly larger which may be a result of the increased water content in the IMS when using water as a solvent in the electrospray. However, the variation is almost within the data spacing of the associated IMS traces (ca. 0.05 ms).

There are some general trends evolving from the data which follow those outlined above for the dications. Thus, monocations with low coordination numbers show a large amount of adduct formation in the mobility cell. An extreme example is the diatomic $NiCl^+$ dication, for which only a fraction below 1% remains unassociated, while the spectrum is dominated by the water adducts $[(H_2O)_nNiCl]^+$ with n = 1–3. In turn, the monocations with larger coordination numbers show a large amount of dissociation upon injection into the mobility unit, e.g. more than 90% CID for the ions $[(CH_3CN)_3Ni]^+$, $[(CH_3CN)_3NiOH]^+$ and $[(CH_3CN)_3NiCl]^+$, respectively. In the

TABLE II

Summarized results from the ion-mobility studies of mass-selected $[(CH_3CN)_nNiX]^{+/2+}$ mono- and dications (n = 0–5; X = OH, Cl, none) generated from a 10^{-3} M solution of $NiCl_2$ in water/acetonitrile (2:1) with the molar fractions[a] x_i of the parent ion, the ionic fragments formed by loss of acetonitrile[b], the adducts due to association with water, and the monocations $[(CH_3CN)_{n'}NiOH]^+$ formed via proton transfer[c,d] in the mobility cell. Further, the arrival times t_a (in ms) of the mass-selected parent ions are given

Parent ion	n	m/z	x_{parent}	x_{CID}[b]	x_{ass}	x_{PT}[c,d]	t_a
$[(CH_3CN)_nNi]^{2+}$[d]	2	70.0[e]	–[e]	–[e]	–[e]	–[e]	5.69[e]
	3	90.5	0.57	0.09	0.30	0.04	5.43
	4	111.0	0.25	0.71		0.04	5.15
	5	131.5	0.01	0.96		0.03	6.03
$[(CH_3CN)_nNi(H_2O)]^{2+}$	3	99.5	0.31	0.64	0.01	0.04	5.43
$[(CH_3CN)_nNiOH]^+$	1	116.0	0.77	0.01	0.22	–[d]	6.73
	2	157.0	0.47	0.52	0.01	–[d]	7.22
	3	198.0	0.02	0.98		–[d]	8.93
$[(CH_3CN)_n(H_2O)NiOH]^+$	1	136.0[f]	0.30	0.70		–[d]	6.77
$[(CH_3CN)_nNiCl]^+$	0	93.0	0.01		0.99	–[d]	8.01
	1	136.0[f]	0.18	0.01	0.81	–[d]	7.92
	2	175.0	0.72	0.20	0.08	–[d]	8.46
	3	216.0	0.06	0.94		–[d]	10.45
$[(CH_3CN)_n(H_2O)NiCl]^+$	1	152.0	0.68	0.19	0.13	–[d]	7.92
$[(CH_3CN)_n(H_2O)_2NiCl]^+$	1	170.0	0.04	0.96		–[d]	8.03
$[(CH_3CN)_nNi]^+$	1	99.0	0.06	0.02	0.92[g]	–[d]	6.29
	2	140.0	0.20	0.80		–[d]	6.46
	3	181.0	0.09	0.91		–[d]	8.39
$[(CH_3CN)_n(H_2O)Ni]^+$	1	117.0	0.80	0.17[g]	0.03	–[d]	6.29
	2	158.0	0.02	0.98		–[d]	7.52

[a] Molar fractions with $\Sigma x_i = 1$. [b] This column includes exchange of one acetonitrile ligand by water. [c] For all ions, the predominating product of hydrolysis is $[(CH_3CN)NiOH]^+$ (m/z 116). [d] Column does not apply for monocation precursors. [e] This ion is not generated in the source in the presence of water. The arrival time is converted from Table I by reference to that of m/z 111.0. [f] ^{60}Ni isotope selected due to overlapping dications for ^{58}Ni. [g] Includes adduct with N_2 at m/z 127.0.

case of the monoligated $[(CH_3CN)Ni]^+$ cation as well as for $[(CH_3CN)Ni(H_2O)]^+$, we further note the formation of a significant amounts of an adduct with nitrogen at *m/z* 127 (i.e. $[(CH_3CN)Ni(N_2)]^+$, m_{exp} = 126.9689, m_{calc} = 126.9680). The observation of this particular nitrogen adduct is consistent with the preferential coordination of N_2 by low-valent transition metals in the gas phase as well as condensed media[47–49], whereas the formal nickel(II) species, e.g. $NiCl^+$, are harder acids and thus prefer coordination to water. Notwithstanding, the observation of N_2 complexes underlines the non-negligible interactions of the ions under study with the nitrogen gas serving as collision partner in the ion-mobility separation.

Finally, let us inspect the arrival times in some more detail. Figure 4 summarizes the arrival times for all nickel species studied in this work. Most of the t_a values show the expected dependence from the *m/z* values as indicated by the diagonal grey rectangular in Fig. 4. However, the species with low coordination numbers (the latter are indicated close to the symbols in Fig. 4) show significantly larger arrival times and hence smaller mobilities than expected from their mere mass. As demonstrated by the graph, this effect is not at all unique to a certain type of ions, but appears as a general

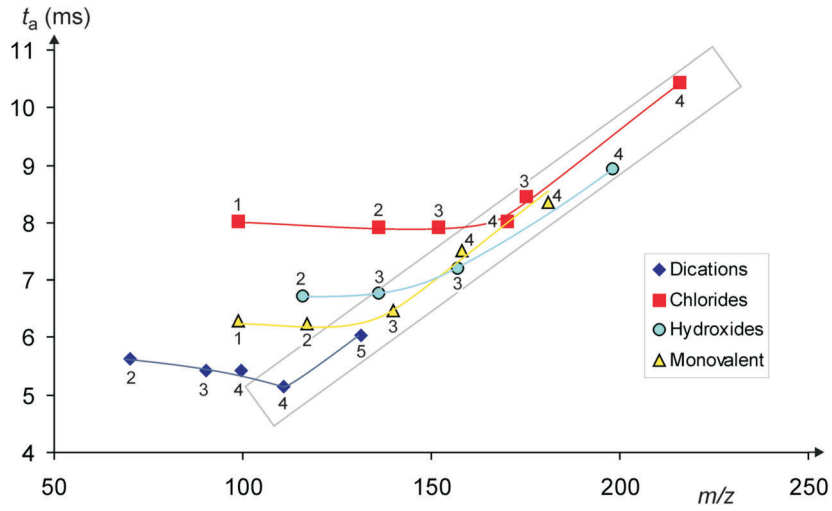

FIG. 4

Arrival times t_a (in ms) of all ions listed in Table II as a function of their mass-to-charge ratios under identical conditions. Linear regression of the points within the grey rectangular gives t_a = (0.0475 *m/z* – 0.07) ms with r^2 = 0.976. The numbers close to the symbols indicate the formal coordination numbers of the ionic species, where the ligand count includes the anionic ligands (e.g. 1 for $NiCl^+$, 2 for $[(CH_3CN)_2Ni]^{2+}$, 3 for $[(CH_3CN)_2NiOH]^+$, etc.)

phenomenon of the nickel complexes with low coordination numbers. For example, t_a of the biscoordinated dication $[(CH_3CN)_2Ni]^{2+}$ is larger than those of $[(CH_3CN)_3Ni]^{2+}$ and $[(CH_3CN)_4Ni]^{2+}$ and likewise the monocations $[(CH_3CN)Ni]^{2+}$, $[(CH_3CN)NiOH]^{+}$, and $[(CH_3CN)NiCl]^{+}$ have much larger arrival times than expected from their masses. This results in a behavior which follows the expected dependence from the *m/z* value for larger coordination numbers and then reaches a plateau-type region for the low-coordinated ions. Qualitatively, this observation can be understood by the formation of transient associates either with background water or with the nitrogen present in the mobility cell which are of higher mass and hence smaller mobility.

To a first approximation, the deviation from the expected linear dependence of *m/z* value and t_a seems to show a correlation with the amount of association observed. To illustrate this effect, in Fig. 5 the deviation of the measured arrival times from the expected values based on the *m/z* values is plotted against the amount of association x_{ass} (Table II). The trend in Fig. 5 is thus consistent with the proposed formation of transient complexes within the mobility cell.

So far, we have learned a lot about the ion-mobility experiment for microsolvated ions, but yet it remains the justified question what information can be extracted from the mobility data about the ions themselves. At first, the results demonstrate the almost trivial finding that low-coordinated nickel species are more reactive and show a higher tendency for association. Vice versa, the larger ions are more likely to undergo collision-induced dissociation. However, there is some additional information which can be

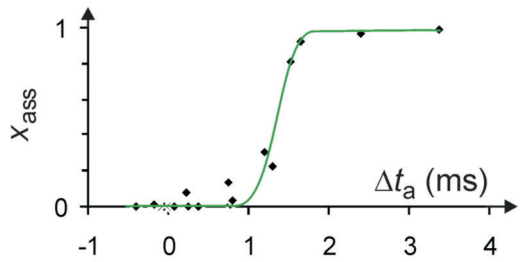

FIG. 5
Deviation of the arrival times Δt_a as determined from the measured values and those derived from a linear fit of the data in the grey square box in Fig. 4 as a function of the amount of association with water. The green sigmoid line does not result from a fit, but should only guide the eyes. Note that due to the definition of x_{ass}, its range is $0 \le x_{ass} \le 1$

derived from the results. Upon inspecting Fig. 4 it is obvious that the ions belong to "families" which follow common trends, reaching different plateau values. For example, the hydroxo complexes converge to arrival times slightly below 7 ms for the lowest coordination numbers, whereas the chloro complexes converge at about 8 ms. This may in fact appear surprising, because chloride is often quoted as the best mimic for hydroxo ligands in (neutral) metal complexes[50]. In fact, an effect due to the net Coulomb charge of the gaseous cations is likely to be the reason for the violation of this otherwise useful analogy. Specifically, the larger arrival times of the cationic chloro complexes can be ascribed to the higher effective charge of the metal atom compared to the cationic hydroxo complexes in which the OH-proton can carry part of the net positive charge[25,26,51–54]. As a result, the electrophilicity of the metal center in a given $[L_nNiOH]^+$ species is lower than that in the corresponding $[L_nNiCl]^+$ ion with the consequence that the association with the gases in the mobility cell is more pronounced for the chloro complexes. This deduction finds direct support in the data of Table II which show much more pronounced association in the cases of the chloro complexes $[(CH_3CN)NiCl]^+$ and $[(CH_3CN)_2NiCl]^+$ (x_{ass} = 0.81 and 0.08, respectively) compared to the analogous hydroxo complexes $[(CH_3CN)NiOH]^+$ and $[(CH_3CN)_2NiOH]^+$ (x_{ass} = 0.22 and 0.01, respectively). The mobility data reported here thereby provide a direct experimental indication for the differential electrophilicity of the metal-ion cores, which so far could only indirectly be derived from thermodynamic data or theoretical calculations[25,26,51–55].

CONCLUSIONS

Ion-mobility mass spectrometry (IM-MS) is applied to a series of cationic nickel complexes with acetonitrile. The choice of this reasonably coherent set of ions provides some fundamental insight into the value of ion-mobility studies for the investigation of microsolvated ions. Inter alia, the present study demonstrates that it is possible to achieve useful information about the coordination properties of medium-sized metal complexes using IM-MS. Moreover, a conceptional model for the understanding of reactive events occurring within the mobility unit is outlined. Two obvious challenges identified for future research are (i) the association of reactive metal species with background impurities, which are in part difficult to avoid because some of them stem from the solutions used as precursors, and (ii) the partial or even complete dissociation of more labile coordination complexes upon injection into the ion-mobility unit.

For low-coordinated nickel complexes, the ion mobilities significantly deviate from the common dependence from the mass-to-charge ratio and are instead larger than expected. This anomaly is ascribed to the formation of transient associates with the gases present in the mobility cell, some of which are also detected experimentally, e.g. $[(CH_3CN)_3Ni(H_2O)_2]^{2+}$ and $[(CH_3CN)Ni(N_2)]^+$. In addition to the information gained about the ion-mobility experiment itself, the present study provides experimental evidence for the conception that in cationic hydroxo complexes the HO proton carries a significant amount of the positive charge which leads to a decrease of the electrophilicity of the metal-ion core.

This work was supported by the European Research Council (AdG HORIZOMS) and the Czech Academy of Sciences (Z40550506).

REFERENCES

1. Rulíšek L., Havlas Z.: *J. Phys. Chem. A* **1999**, *103*, 1634.
2. Rulíšek L., Havlas Z.: *J. Chem. Phys.* **2000**, *112*, 149.
3. Rulíšek L., Havlas Z.: *J. Am. Chem. Soc.* **2000**, *122*, 10428.
4. Rulíšek L., Havlas Z.: *J. Phys. Chem. A* **2002**, *106*, 3855.
5. Rulíšek L., Havlas Z.: *Int. J. Quantum Chem.* **2003**, *91*, 504.
6. Rulíšek L., Havlas Z.: *J. Phys. Chem. B* **2003**, *107*, 2376.
7. Schröder D., Schwarz H.: *J. Phys. Chem. A* **1999**, *103*, 7385.
8. Schröder D.: *Angew. Chem. Int. Ed.* **2004**, *43*, 1329.
9. Roithová J., Schröder D.: *Phys. Chem. Chem. Phys.* **2007**, *9*, 2341.
10. Fenn J. B.: *Angew. Chem. Int. Ed.* **2003**, *42*, 3871.
11. Cheng Z. L., Siu K. W. M., Guevremont R., Berman S. S.: *Org. Mass Spectrom.* **1992**, *27*, 1370.
12. Kohler M., Leary J. A.: *J. Am. Soc. Mass Spectrom.* **1997**, *8*, 1124.
13. Kohler M., Leary J. A.: *Int. J. Mass Spectrom.* **1997**, *162*, 17.
14. Seto C., Stone J. A.: *Int. J. Mass Spectrom.* **1998**, *175*, 263.
15. Shvartsburg A. A., Wilkes J. G., Lay J. O., Siu K. W. M.: *Chem. Phys. Lett.* **2001**, *350*, 216.
16. Combariza M. Y., Vachet R. W.: *J. Am. Soc. Mass Spectrom.* **2002**, *13*, 813.
17. Combariza M. Y., Vachet R. W.: *J. Phys. Chem. A* **2004**, *108*, 1757.
18. Combariza M. Y., Vachet R. W.: *J. Am. Soc. Mass Spectrom.* **2004**, *15*, 1128.
19. Combariza M. Y., Fermann J. T., Vachet R. W.: *Inorg. Chem.* **2004**, *43*, 2745.
20. Combariza M. Y., Fahey A. M., Milshteyn A., Vachet R. W.: *Int. J. Mass Spectrom.* **2005**, *244*, 109.
21. Xiao C. Y., Walker K., Hagelberg F., El-Nahas A. M.: *Int. J. Mass Spectrom.* **2004**, *233*, 87.
22. Shvartsburg A. A.: *Chem. Phys. Lett.* **2002**, *360*, 479.
23. Stace A. J.: *J. Phys. Chem. A* **2002**, *106*, 7993.
24. Marcus Y., Hefter G.: *Chem. Rev.* **2006**, *106*, 4585.
25. Tsierkezos N. G., Roithová J., Schröder D., Ončák M., P. Slavíček P.: *Inorg. Chem.* **2009**, *48*, 6287.

26. Ducháčková L., Roithová J., Milko P., Žabka J., Tsierkezos N., Schröder D.: *Inorg. Chem.* **2011**, *50*, 771.
27. Cech N. B., Enke C. G.: *Mass Spectrom. Rev.* **2001**, *20*, 362.
28. Trage C., Diefenbach M., Schröder D., Schwarz H.: *Chem. Eur. J.* **2006**, *12*, 2454.
29. Jagoda-Cwiklik B., Jungwirth P., Rulíšek L., Milko P., Roithová J., Lemaire J., Maitre P., Ortega J. M., Schröder D.: *ChemPhysChem* **2007**, *8*, 1629.
30. Cooper T., O'Brien J. T., Williams E. R., Armentrout P. B.: *J. Phys. Chem A* **2010**, *114*, 12646.
31. Schröder D., Schwarz H.: *Can. J. Chem.* **2005**, *83*, 1936.
32. Schröder D., Roithová J., Schwarz H.: *Int. J. Mass Spectrom.* **2006**, *254*, 197.
33. For a recent review of the gas-phase chemistry of nickel-containing cations, see: Mó O., Yañez M., Salpin J. Y., Tortajada J.: *Mass Spectrom. Rev.* **2007**, *26*, 474.
34. Kanu A. B., Dwivedi P., Tam M., Matz L., Hill H. H.: *J. Mass Spectrom.* **2007**, *43*, 1.
35. Bohrer B. C., Mererbloom S. I., Koeniger S. L., Hilderbrand A. E., Clemmer D. E.: *Ann. Rev. Anal. Chem.* **2008**, *1*, 293.
36. Puton J., Nousiainen M., Sillanpaa M.: *Talanta* **2008**, *76*, 978.
37. Pringle S. D., Giles K., Wildgoose J. L., Williams J. P., Slade S. E., Thalassinos K., Baterman R. H., Bowers M. T., Scrivens J. H.: *Int. J. Mass Spectrom.* **2007**, *261*, 1.
38. Révész Á., Schröder D., Rokob T. A., Havlik M., Dolenský B.: *Angew. Chem. Int. Ed.* **2011**, *50*, 2401.
39. D'Agostino P. A., Chenier C. L.: *Rapid Commun. Mass Spectrom.* **2010**, *24*, 1617.
40. Cooper T. E., Armentrout P. B.: *J. Phys. Chem. A* **2009**, *113*, 13742.
41. Roithová J., Schröder D.: *Phys. Chem. Chem. Phys.* **2007**, *9*, 731.
42. Fernández-Maestre R., Wu C., Hill H. H., Jr.: *Int. J. Mass Spectrom.* **2010**, *298*, 2.
43. Kebarle P., Peschke M.: *Anal. Chim. Acta* **2000**, *406*, 11.
44. Tsierkezos N., Schröder D., Schwarz H.: *J. Phys. Chem. A* **2003**, *107*, 9575.
45. Tsierkezos N. G., Schröder D., Schwarz H.: *Int. J. Mass Spectrom.* **2004**, *235*, 33.
46. For a unambiguous proof of this concept for a series of copper(II) ions, see: a) Schröder D., Weiske T., Schwarz H.: *Int. J. Mass Spectrom.* **2002**, *219*, 729; b) Milko P., Roithová J., Schröder D., Lemaire J., Schwarz H., Holthausen M. C.: *Chem. Eur. J.* **2008**, *14*, 4318; c) Tintaru A., Charles L., Milko P., Roithová J., Schröder D.: *J. Phys. Org. Chem.* **2009**, *22*, 229; d) Tsierkezos N. G., Buchta M., Holý P., Schröder D.: *Rapid Commun. Mass Spectrom.* **2009**, *23*, 1550; e) Révész Á., Milko P., Žabka J., Schröder D., Roithová J.: *J. Mass Spectrom.* **2010**, *45*, 1246; f) Jaklová Dytrtová J., Jakl M., Schröder D., Čadková E., Komárek M.: *Rapid Commun. Mass Spectrom.* **2011**, *25*, 1037.
47. For gas-phase studies of N_2 complexes with late 3d metal cations, see: a) Khan F. A., Steele D. L., Armentrout P. B.: *J. Phys. Chem.* **1995**, *99*, 7819; b) Schwarz J., Heinemann C., Schwarz H.: *J. Phys. Chem.* **1995**, *99*, 11405; c) Heinemann C., Schwarz J., Schwarz H.: *J. Phys. Chem.* **1996**, *100*, 6088; d) Tjelta B. L., Armentrout P. B.: *J. Phys. Chem. A* **1997**, *101*, 2064; e) Dieterle M., Harvey J. N., Heinemann C., Schwarz J., Schröder D., Schwarz H.: *Chem. Phys. Lett.* **1997**, *277*, 399.
48. Chen M. H., Zhou M. F., Zhang L. N., Qin Q. Z.: *J. Phys. Chem. A* **2000**, *104*, 8627.
49. Toupadakis A., Kubas G. J., King W. A., Scott B. L., Huhmann-Vincent J.: *Organometallics* **1998**, *17*, 5315.
50. Hildenbrand D. L.: *J. Chem. Phys.* **1995**, *103*, 2634.
51. Schröder D., Schwarz H.: *Int. J. Mass Spectrom.* **2003**, *227*, 121.
52. Schröder D.: *J. Phys. Chem. A* **2008**, *112*, 13215.

53. Schröder D., Souvi O., Alikhani E.: *Chem. Phys. Lett.* **2009**, *470*, 162.
54. Ončák M., Schröder D., Slavíček P.: *J. Comp. Chem.* **2010**, *31*, 2294.
55. Schröder D., Ducháčková L., Tarábek J., Karwowska M., Fijalkowski K. J., Ončák M., Slavíček P.: *J. Am. Chem. Soc.* **2011**, *133*, 2444.